Inversion Symmetry Breaking by Oxygen Octahedral Rotations in the Ruddlesden-Popper NaRTiO$_4$ Family

Hirofumi Akamatsu,[1,*] Koji Fujita,[2,†] Toshihiro Kuge,[2] Arnab Sen Gupta,[1] Atsushi Togo,[3] Shiming Lei,[1] Fei Xue,[1] Greg Stone,[1] James M. Rondinelli,[4] Long-Qing Chen,[1] Isao Tanaka,[3] Venkatraman Gopalan,[1,‡] and Katsuhisa Tanaka[2]

[1]*Materials Research Institute and Department of Materials Science and Engineering, Pennsylvania State University, MSC Building, University Park, Pennsylvania 16802, USA*

[2]*Department of Material Chemistry, Kyoto University, Nishikyo, Kyoto 615-8510, Japan*

[3]*Department of Materials Science and Engineering, Kyoto University, Sakyo, Kyoto 606-8501, Japan*

[4]*Department of Materials Science and Engineering, Drexel University, Philadelphia, Pennsylvania 19104, USA*

(Received 20 January 2014; published 7 May 2014)

Rotations of oxygen octahedra are ubiquitous, but they cannot break inversion symmetry in simple perovskites. However, in a layered oxide structure, this is possible, as we demonstrate here in A-site ordered Ruddlesden-Popper NaRTiO$_4$ (R denotes rare-earth metal), previously believed to be centric. By revisiting this series via synchrotron x-ray diffraction, optical second-harmonic generation, piezoresponse force microscopy, and first-principles phonon calculations, we find that the low-temperature phase belongs to the acentric space group $P\bar{4}2_1m$, which is piezoelectric and nonpolar. The mechanism underlying this large new family of acentric layered oxides is prevalent, and could lead to many more families of acentric oxides.

DOI: 10.1103/PhysRevLett.112.187602 PACS numbers: 77.65.-j, 42.70.Mp, 61.05.C-, 63.20.dk

Acentric materials are under intense investigation owing to their fascinating properties, including piezoelectricity and nonlinear optical effects. Perovskite oxides without inversion symmetry are widely used as capacitors and transducers. In the acentric perovskites, structural distortions leading to the noncentrosymmetry are driven by second-order Jahn-Teller (SOJT) active cations such as Ti^{4+}, lone pair electrons as in Pb^{2+}, or a small tolerance factor resulting in lithium niobate-type structures [1–4]. This fact limits the abundance of acentric systems to less than 5% of all known perovskite oxides [5]. Moreover, in low-dimensional systems like layered perovskites, the two dimensionality can suppress the coherence of such cooperative distortions and thereby decouples the subunits from each other, which further limits the abundance of acentric systems [6,7].

In this Letter, we report noncentrosymmetry in layered perovskites, NaRTiO$_4$ (R denotes rare-earth metal), induced by oxygen octahedral rotations (OORs), which are ubiquitous distortions in perovskite-related compounds [8]. Fascinating ideas on creating noncentrosymmetry in layered perovskites by means of OORs have been recently suggested by theory [9–15]. Some types of OORs can remove inversion centers at the A sites but not at the B sites in ABO_3 perovskites. Rondinelli and Fennie [12] proposed double perovskites with layered A-site-cation ordering $AA'B_2O_6$, which lack inversion symmetry at the B sites due to the cation ordering, and at the A and A' sites due to OORs represented by $a^-a^-c^+$ in Glazer notation [16]. Another way to remove inversion centers at the B sites is to employ naturally occurring layered perovskites such as Ruddlesden-Popper (RP), Dion-Jacobsen, Aurivillius phases, and [110]-layered perovskites [10,11,13,17], most of which are readily made by conventional solid-state reactions and, in some cases, a subsequent topochemical process [18]. Benedek *et al.* [10,11] have discussed $n = 2$ RP phases $Ca_3B_2O_7$ (B = Ti, Mn). In the high-symmetry structure of the $n = 2$ RP phase, which has no OORs, the inversion centers exist not at the B sites but at the A sites in the perovskite layers and between the A sites in the rocksalt layers. The $a^-a^-c^+$-type of OORs in the perovskite blocks remove these inversion centers. The above two examples are classified as hybrid improper ferroelectrics. Theory has revealed [10,11,15,17] and predicted [11–14,19] noncentrosymmetry with the origin related to OORs for several layered perovskites but there are no experimental reports clearly demonstrating the acentric-to-centric phase transitions caused by OORs to our knowledge, although the low-temperature acentric structures have been identified for some of the layered perovskites based on diffraction methods [20–22].

Here we report an experimental and theoretical study of an A-site-ordered $n = 1$ RP series, NaRTiO$_4$, revealing that the inversion symmetry is broken by OORs. As shown in Fig. 1(a), a simple $n = 1$ RP phase A_2BO_4 possesses inversion centers at the B sites and between the A sites [11,14]. These inversion centers at the B sites are removed in the A-site-ordered $n = 1$ RP structure with $P4/nmm$ space group [Fig. 1(b)]. The remaining inversion centers can be removed by OORs as shown in Fig. 1(c) [11,14]. However, the noncentrosymmetry has not been experimentally reported for any A-site-ordered $n = 1$ RP phase such as $ARTiO_4$ (A = H, Li, Na, K, Ag) [14,23–30]. The previous articles have reported that some of the RP phases exhibit $a^-a^-c^0$-type of OORs, leaving them centric (space group: $Pbcm$). In this study, however, we have revisited the NaRTiO$_4$ series to find that NaRTiO$_4$ exhibits a phase

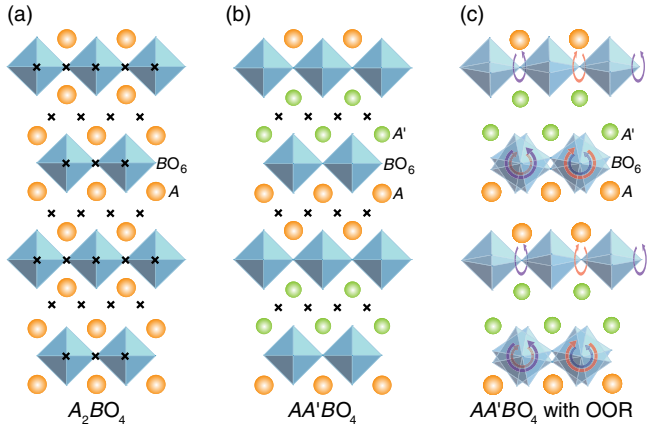

FIG. 1 (color online). Schematics of (a) an $n = 1$ RP phase A_2BO_4 [$I4/mmm$], (b) an $n = 1$ RP phase with layered A-site-cation ordering $AA'BO_4$ [$P4/nmm$], and (c) $AA'BO_4$ with $a^-b^0c^0/b^0a^-c^0$-type octahedral rotations [$P\bar{4}2_1m$]. The cross symbols indicate the locations of inversion centers.

transition from $P4/nmm$ into $P\bar{4}2_1m$ accompanying $a^-b^0c^0/b^0a^-c^0$-type OORs [Fig. 1(c)]. Here, $P\bar{4}2_1m$ is acentric but nonpolar. This is a rare example for the acentric $n = 1$ RP oxides; $LaSrLi_{0.5}Ru_{0.5}O_4$ is the only acentric $n = 1$ RP oxide reported experimentally to the best of our knowledge [31], and the synthesis of Pb_2TiO_4, which has been predicted to be acentric [32], has not been reported yet.

First-principles calculations were performed for NaRTiO$_4$ to determine OOR patterns that lower the total energy of the parent $P4/nmm$ structure [Fig. 1(b)]. Our calculations were carried out using the projector augmented-wave method [33,34] and the PBEsol functional [35–37] as implemented in the VASP code [38–41]. The phonon band structures were derived from the calculated force constants using the PHONOPY code [42] to explore stable structures systematically [43]. (See Supplemental Material for details [44].) The phonon band structures between Γ and M are shown for NaRTiO$_4$ with R = La and Y in Figs. 2(a) and 2(b), respectively. Two doubly degenerate imaginary modes, which transform like the irreducible representations (irreps) M_1 and M_2, are found at M for $NaYTiO_4$, while both modes are stable for $NaLaTiO_4$. We calculated the total energies of $NaYTiO_4$ with the structures in which the atoms were moved according to a set of linear combinations of the calculated M_1 mode eigendisplacements [Fig. 2(c)]. The space groups of the obtained structures, i.e., isotropy subgroups [45], are $P4/nmm$ (the origin), $P\bar{4}2_1m$ (the horizontal and vertical axes other than the origin), $Pbcm$ (the diagonal lines of other than the origin), and $P2_12_12$ (all regions other than those mentioned above). The M_1 modes leading to the $Pbcm$, $P\bar{4}2_1m$, and $P2_12_12$ structures are denoted as $M_1(\eta_1, 0)$, $M_1(\eta_1, \eta_1)$, and $M_1(\eta_1, \eta_2)$ modes, respectively, where (η_1, η_2) is a general order parameter direction in the subspace defined by irrep M_1 [14,45]. The (η_1, 0) and (η_1, η_1) directions are illustrated in Fig. 2(c). We found the total-energy minima for the $P\bar{4}2_1m$ structure in the subspace. The atomic

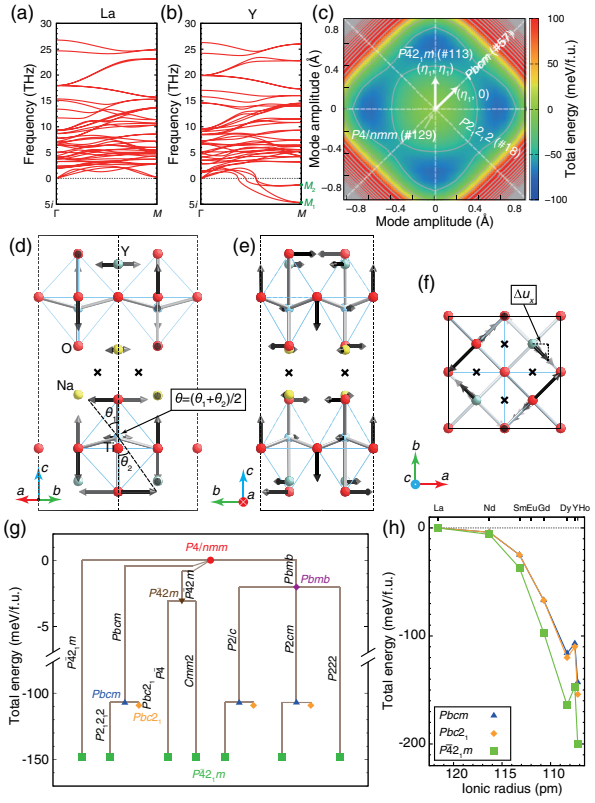

FIG. 2 (color online). Phonon band structures between the $\Gamma(000)$ and $M(\frac{1}{2}\frac{1}{2}0)$ points for NaRTiO$_4$ with parent $P4/nmm$ structures for R = (a) La and (b) Y. (c) Total energies of $NaYTiO_4$ mapped on the subspace spanned by linear combinations of the degenerated M_1 modes. Atomic displacement patterns of the $M_1(\eta_1, \eta_1)$ mode viewed from the (d) [110], (e) [100], and (f) [001] directions are schematically illustrated as arrows on the $P4/nmm$ structure. The cross marks indicate the locations of inversion centers in the $P4/nmm$ structure. (g) Treelike line diagram of $NaYTiO_4$ [see text for details]. (h) Total energies of the $Pbcm$, $Pbc2_1$, and $P\bar{4}2_1m$ structures for NaRTiO$_4$ R = La, Nd, Sm, Gd, Dy, Y, and Ho) relative to that of the $P4/nmm$ structures.

displacements for the $M_1(\eta_1, \eta_1)$ mode are illustrated as arrows superposed on a $\sqrt{2} \times \sqrt{2} \times 1$ supercell of the $P4/nmm$ structure in Figs. 2(d)–2(f). The $M_1(\eta_1, \eta_1)$ mode involves OORs represented by $a^-b^0c^0/b^0a^-c^0$, while the $M_1(0, \eta_1)$ mode corresponds to $a^-a^-c^0$-type OORs. Total energies of the $P\bar{4}2_1m$ and $Pbcm$ structure relative to the $P4/nmm$ structure are -148 meV/f.u. and -107 meV/f.u., respectively, after the lattice constants and atomic coordinates are fully relaxed under the constraint of the symmetry. A treelike line diagram schematizing the results of the stable-structure search within $\sqrt{2} \times \sqrt{2} \times 1$ cell doubling against the $P4/nmm$ structure is shown in Fig. 2(g), where the space groups of the structures obtained by freezing the imaginary modes for the parent structures and those of the structures fully relaxed after the freezing are seen along the lines and at the symbols, respectively. As a result, we found that the $P\bar{4}2_1m$ and $Pbc2_1$ structures are the two dynamically stable structures remaining within this stable-structure search and that the $P\bar{4}2_1m$ structure

is the most stable. Total-energy calculations of NaRTiO$_4$ (R = Y, La-Ho) with $P4/nmm$, $P\bar{4}2_1m$, $Pbcm$, and $Pbc2_1$ structures [Fig. 2(h)] revealed that the $P\bar{4}2_1m$ structures were the most stable except for R = La, where the $P\bar{4}2_1m$, $Pbcm$, and $Pbc2_1$ structures relaxed to the $P4/nmm$ structure. The energy difference between the $P\bar{4}2_1m$ and $P4/nmm$ structures becomes larger with a decrease in the ionic radius of the R ions, r_R [46], possibly because the OOR is driven by the coordination preference of the A-site cations as in perovskite-related compounds. There is a small deviation from this tendency between Dy and Y likely because Y is one of the fifth-period R elements and chemically different from the other sixth-period R elements; the R-O covalent bonds are considered to be attributed to Y $4d$, $5s$–O $2p$ interactions for NaYTiO$_4$, and R $5d$, $6s$–O $2p$ interactions for the others.

Thus, the first-principles calculations have predicted acentric $P\bar{4}2_1m$ structures as the ground states for small R ions. The inversion centers in the $P4/nmm$ structure are removed by the zone-boundary $M_1(\eta_1,\eta_1)$ OOR mode accompanying a $\sqrt{2}\times\sqrt{2}\times 1$ cell doubling [47]. A recent group-theoretical analysis has indicated the possibility of this kind of centric-to-acentric phase transition path [14]. However, the centric $Pbcm$ structures have been experimentally reported so far [29,48,49]. Therefore, we reinvestigated the structures experimentally as follows.

Polycrystalline NaRTiO$_4$ samples were synthesized via conventional solid-state reactions [see the inset of Fig. 4(a)]. Our synthesis conditions are similar to those reported in Ref. [29] and are described in the Supplemental Material [44]. To reinvestigate the structures of the compounds, high-resolution synchrotron x-ray diffraction (SXRD) patterns were taken with a Debye-Scherrer camera at the BL02B2 beam line of SPring-8. Figure 3(a) depicts the room temperature (RT) SXRD patterns for R = Y, La-Ho. The SXRD patterns for R = La and Nd show tetragonal symmetry with a systematic absence of the $hk0$ reflections for $h+k=2n+1$ [29]. Taking into account the extinction rule and assuming that they exhibit $n=1$ RP structures, the plausible structures are the A-site-cation ordered $n=1$ RP phases with $P4/nmm$ space group shown in Fig. 1(b) [29]. A Rietveld refinement (see Supplemental Material [44]) of the SXRD pattern for R = La using the RIETAN-FP code [50] showed a small weighted-profile reliability factor ($R_{\rm WP}=5.341$), while a refinement for R = Nd resulted in considerable reliability factor ($R_{\rm WP}=12.159$), partly because it undergoes a phase transition to an acentric phase just below RT, as revealed later. Superlattice reflection peaks corresponding to a $\sqrt{2}\times\sqrt{2}\times 1$ cell doubling are found in the SXRD patterns for R = Y, Sm-Ho at RT [the inset of Fig. 3(a)]. The superlattice reflection peak for R = Sm diminishes at high temperatures around 800 K as shown in the Supplemental Material [44], indicating a phase transition between $P4/nmm$ and lower-symmetry phases. The tetragonal $P\bar{4}2_1m$ and orthorhombic $Pbcm$ and $Pbc2_1$ space groups have been derived from the extinction rule and the compatibility with $n=1$ RP structures [51]. The SXRD patterns fit

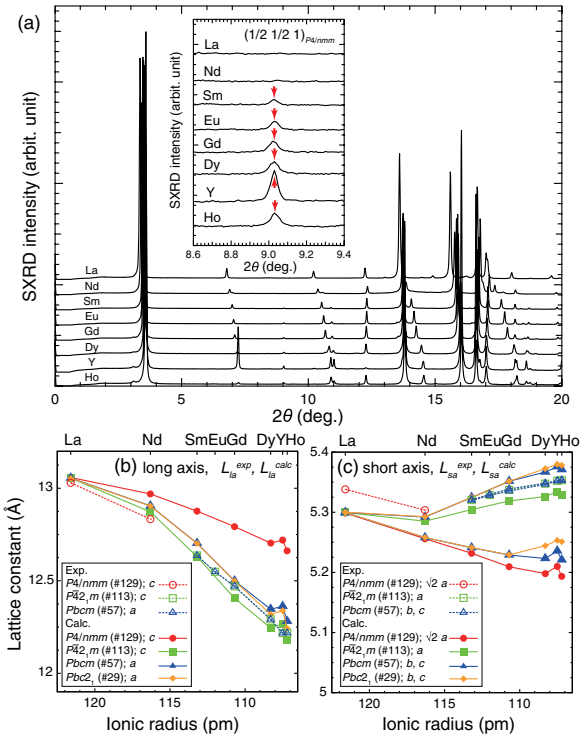

FIG. 3 (color online). (a) SXRD patterns at RT for NaRTiO$_4$ with R = La, Nd, Sm, Eu, Gd, Dy, Y, Ho (top to bottom). The inset of (a) shows an enlarged view of the region around the $(\frac{1}{2}\frac{1}{2}1)$ superlattice reflection peaks. Experimental and calculated (b) long- and (c) short-axis lattice constants plotted against r_R.

well using the $P\bar{4}2_1m$ structural model with a small reliability factor ($R_{\rm WP}=5.652$ for R = Y) that is very similar to those found in the refinement based on the $Pbcm$ ($R_{\rm WP}=6.289$) and $Pbc2_1$ ($R_{\rm WP}=5.722$) models. Thus, we cannot unambiguously determine the structure only in terms of the reliability factors in the Rietveld analysis of the SXRD data, likely because of the difficulty refining the oxygen positions.

As shown below, however, the dependence of lattice constants on r_R along with the optical second-harmonic generation (SHG) and piezoresponse force microscopy (PFM) provides unequivocal experimental evidence for the $P\bar{4}2_1m$ structure. Figures 3(b) and 3(c) illustrate the experimental (exp) and calculated (calc) long- (la) and short-axis (sa) lattice constants, L. There are two interesting findings concerning $L_{\rm sa}^{\rm exp}$ and $L_{\rm sa}^{\rm calc}$: First, the pairs of $L_{\rm sa}^{\rm exp}$ obtained using the orthorhombic $Pbcm$ model are similar to each other, i.e., $b\simeq c$ for R = Y, Sm-Ho, indicating tetragonality, in contrast to the pairs of $L_{\rm sa}^{\rm calc}$ for $Pbcm$ and $Pbc2_1$, where b and c diverge as r_R becomes smaller. Secondly, the $L_{\rm sa}^{\rm exp}$ shows an upturn between Nd and Sm, where the superlattice reflections emerge. This behavior is well reproduced by $L_{\rm sa}^{\rm calc}$ for $P\bar{4}2_1m$. Thus, these results clearly support the $P\bar{4}2_1m$ structures and rule out the $Pbcm$ and $Pbc2_1$ structures for R = Y, Sm-Ho.

Both optical SHG and PFM are sensitive probes of noncentrosymmetry because the probed properties are related to third-rank polar tensor [52]. Optical SHG measurements were performed in reflection geometry with

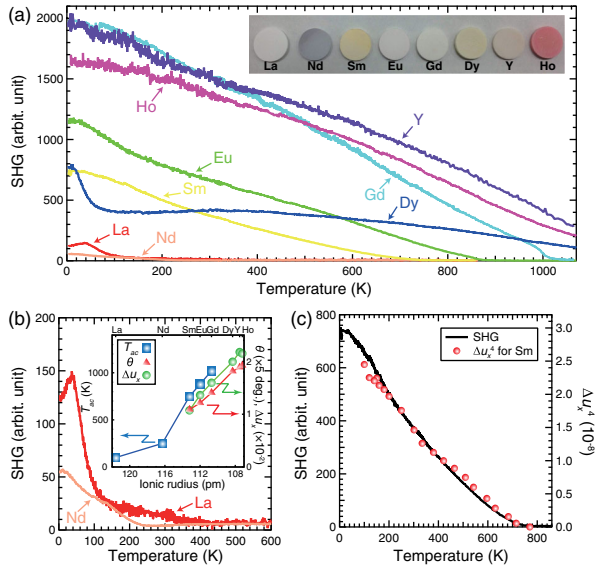

FIG. 4 (color online). (a) Temperature dependence of SHG intensity for NaRTiO$_4$ with R = La, Nd, Sm, Eu, Gd, Dy, Y, Ho. (b) Magnified view of the low intensity region. The inset of (b) shows the acentric-to-centric phase transition temperature T_{ac}, OOR angle θ, and displacement of R ions in the x direction Δu_x, illustrated in Fig. 2(f) as a function of r_R. (c) Temperature dependence of SHG and Δu_x^4 for $R = Sm$. The inset of (a) shows the NaRTiO$_4$ pellet samples.

an 800 nm fundamental beam (Ti:sapphire laser, 80 fs pulses, 1 kHz repetition rate). Figure 4(a) shows that finite SHG signals are observed at RT for NaRTiO$_4$ with R = Y, Sm-Ho, which exhibits superlattice reflections in the RT SXRD patterns [the inset of Fig. 3(a)]. These results clearly support the acentric $P\bar{4}2_1m$ structure over the centric $Pbcm$ structure at RT. The SHG signal for R = Sm diminishes at about 800 K where its x-ray superlattice reflection peaks disappear [44]. Note that in this series, the single nonpolar mode, i.e., $M_1(\eta_1, \eta_1)$ mode, breaks the inversion symmetry, which is similar to a K_3 mode in an improper ferroelectric $YMnO_3$ [53,54] although this series is nonpolar [55], and, thereby, the cell doubling due to the OOR occurs just at a acentric-to-centric phase transition temperature, T_{ac} [56]. The centric-to-acentric transitions were observed for Sm, Eu, and Gd above RT. The T_{ac}'s are higher than 1073 K for R = Dy, Y, and Ho. The enlargement of the low intensity region is shown in Fig. 4(b). The acentric-to-centric transitions are observed at 100 and 270 K for R = La and Nd, respectively, indicating that they also crystalize to $P\bar{4}2_1m$ structure at low temperatures. For R = La, the calculated $M_1(\eta_1, \eta_1)$ phonon modes are stable but the frequency is almost zero [see Fig. 2(a)]; that is, the calculation predicts that it is on the verge of a soft-mode transition. Such a subtle difference between the experiment and theory may arise partly because of the employed functional. The inset of Fig. 4(b) shows that the T_{ac} monotonically increases with a decrease in r_R, in good agreement with the calculation results that the smaller the r_R, the more favored the $P\bar{4}2_1m$ phase is [see Fig. 2(h)].

The OOR angle θ and displacement of rare-earth metal ions in the x direction Δu_x, illustrated in Figs. 2(d) and 2(f), respectively, are considered as a measure of amplitude of the $M_1(\eta_1, \eta_1)$ mode [44]. The inset of Fig. 4(b) plots the r_R dependence of Δu_x and θ obtained from the Rietveld refinements of RT SXRD. As r_R becomes smaller, both Δu_x and θ become larger. Figure 4(c) illustrates that the temperature dependence of the SHG intensity has a similar trend to that of Δu_x^4 as expected from Landau theory [44]. Also for R = Eu and Y, Δu_x^4 shows a good overlap with the SHG intensity [44]. We also performed PFM by using an atomic force microscope system (Bruker, Dimension Icon) for the NaRTiO$_4$ (R = Dy and Ho) pellet samples, and then confirmed their piezoelectricity as shown in the Supplemental Material [44]. The piezoelectric strain coefficients were calculated by using density functional perturbation theory implemented in the VASP code [57,58]. The calculated coefficients become larger with a decrease in r_R [44]. For $P\bar{4}2_1m$ NaYTiO$_4$, $d_{14} = 4.3$, and $d_{36} = 6.0$ pC/N.

In summary, we have uncovered a large family of acentric and piezoelectric RP oxides, NaRTiO$_4$. A novel mechanism for breaking inversion symmetry via OORs in A-site ordered RP phases was reported. The low-temperature phase of this RP series has been shown to belong to acentric $P\bar{4}2_1m$ rather than centric $Pbcm$, as suggested before. This study suggests a need to revisit other A-site-ordered $n = 1$ RP phases including well-studied ARTiO$_4$ (A = H, Li, Na, K, Ag), where we predict a similar mechanism to be active, which could lead to a rich selection of acentric materials.

Authors acknowledge N. A. Benedek for fruitful discussions. The synchrotron radiation experiments were performed at the BL02B2 of SPring-8 with the approval of the Japan Synchrotron Radiation Research Institute (JASRI) (Proposal No. 2011B1504 and No. 2013A1683). This research was supported by Grants-in-Aid for Japan Society of the Promotion of Science (JSPS) Fellowship (No. 22-1280), JSPS Fellowship for Research Abroad (No. 25-185), and Scientific Research (A) (No. 25249090) and by the National Science Foundation (NSF) through Materials Research Science and Engineering Centers (MRSEC) Grants No. DMR-0820404 and No. DMR-1210588.

*hua14@psu.edu
†fujita@dipole7.kuic.kyoto-u.ac.jp
‡vxg8@psu.edu

[1] N. A. Hill, J. Phys. Chem. B **104**, 6694 (2000).
[2] N. A. Benedek and C. J. Fennie, J. Phys. Chem. C **117**, 13 339 (2013).
[3] I. B. Bersuker, Phys. Rev. Lett. **108**, 137202 (2012).
[4] J. M. Rondinelli, A. S. Eidelson, and N. A. Spaldin, Phys. Rev. B **79**, 205119 (2009).

[5] V. L. Karen and M. Hellenbrandt, Acta Crystallogr. Sect. A **58**, c367 (2002).
[6] T. Birol, N. A. Benedek, and C. J. Fennie, Phys. Rev. Lett. **107**, 257602 (2011).
[7] C.-H. Lee *et al.*, Nature (London) **502**, 532 (2013).
[8] M. W. Lufaso and P. M. Woodward, Acta Crystallogr. Sect. B **57**, 725 (2001).
[9] E. Bousquet, M. Dawber, N. Stucki, C. Lichtensteiger, P. Hermet, S. Gariglio, J.-M. Triscone, and P. Ghosez, Nature (London) **452**, 732 (2008).
[10] N. A. Benedek and C. J. Fennie, Phys. Rev. Lett. **106**, 107204 (2011).
[11] N. A. Benedek, A. T. Mulder, and C. J. Fennie, J. Solid State Chem. **195**, 11 (2012).
[12] J. M. Rondinelli and C. J. Fennie, Adv. Mater. **24**, 1961 (2012).
[13] A. T. Mulder, N. A. Benedek, J. M. Rondinelli, and C. J. Fennie, Adv. Funct. Mater. **23**, 4810 (2013).
[14] P. V. Balachandran, D. Puggioni, and J. M. Rondinelli, Inorg. Chem. **53**, 336 (2014).
[15] T. Fukushima, A. Stroppa, S. Picozzi, and J. M. Perez-Mato, Phys. Chem. Chem. Phys. **13**, 12 186 (2011).
[16] A. M. Glazer, Acta Crystallogr. Sect. B **28**, 3384 (1972).
[17] J. López-Pérez and J. Íñiguez, Phys. Rev. B **84**, 075121 (2011).
[18] R. E. Schaak and T. E. Mallouk, Chem. Mater. **14**, 1455 (2002).
[19] J. Young and J. M. Rondinelli, Chem. Mater. **25**, 4545 (2013).
[20] N. Ishizawa, F. Marumo, S. Iwai, M. Kimura, and T. Kawamura, Acta Crystallogr. Sect. B **38**, 368 (1982).
[21] N. Guiblin, D. Grebille, H. Leligny, and C. Martin, Acta Crystallogr. Sect. C **58**, i3 (2002).
[22] G. King, S. Thimmaiah, A. Dwivedi, and P. M. Woodward, Chem. Mater. **19**, 6451 (2007).
[23] S.-H. Byeon, J.-J. Yoon, and S.-O. Lee, J. Solid State Chem. **127**, 119 (1996).
[24] S. Nishimoto, M. Matsuda, S. Harjo, A. Hoshikawa, T. Kamiyama, T. Ishigaki, and M. Miyake, J. Eur. Ceram. Soc. **26**, 725 (2006).
[25] S. Nishimoto, M. Matsuda, S. Harjo, A. Hoshikawa, T. Kamiyama, T. Ishigaki, and M. Miyake, J. Solid State Chem. **179**, 1892 (2006).
[26] G. Blasse, J. Inorg. Nucl. Chem. **30**, 656 (1968).
[27] K. Toda, S. Kurita, and M. Sato, Solid State Ionics **81**, 267 (1995).
[28] K. Toda, S. Kurita, and M. Sato, J. Ceram. Soc. Jpn. **104**, 140 (1996).
[29] K. Toda, Y. Kameo, S. Kurita, and M. Sato, J. Alloys Compd. **234**, 19 (1996).
[30] R. E. Schaak and T. E. Mallouk, J. Solid State Chem. **161**, 225 (2001).
[31] J. A. Rodgers, P. D. Battle, N. Dupré, C. P. Grey, and J. Sloan, Chem. Mater. **16**, 4257 (2004).
[32] C. J. Fennie and K. M. Rabe, Phys. Rev. B **71**, 100102 (2005).
[33] P. E. Blöchl, Phys. Rev. B **50**, 17953 (1994).
[34] G. Kresse and D. Joubert, Phys. Rev. B **59**, 1758 (1999).
[35] J. P. Perdew, K. Burke, and M. Ernzerhof, Phys. Rev. Lett. **77**, 3865 (1996).
[36] J. P. Perdew, K. Burke, and M. Ernzerhof, Phys. Rev. Lett. **78**, 1396 (1997).
[37] J. P. Perdew, A. Ruzsinszky, G. I. Csonka, O. A. Vydrov, G. E. Scuseria, L. A. Constantin, X. Zhou, and K. Burke, Phys. Rev. Lett. **100**, 136406 (2008).
[38] G. Kresse and J. Hafner, Phys. Rev. B **48**, 13115 (1993).
[39] G. Kresse and J. Hafner, Phys. Rev. B **47**, 558 (1993).
[40] G. Kresse and J. Furthmüller, Comput. Mater. Sci. **6**, 15 (1996).
[41] G. Kresse and J. Furthmüller, Phys. Rev. B **54**, 11169 (1996).
[42] A. Togo, F. Oba, and I. Tanaka, Phys. Rev. B **78**, 134106 (2008).
[43] A. Togo and I. Tanaka, Phys. Rev. B **87**, 184104 (2013).
[44] See Supplemental Material at http://link.aps.org/supplemental/10.1103/PhysRevLett.112.187602, which includes Refs. [58–64].
[45] H. T. Stokes and D. M. Hatch, *Isotropy Subgroups of the 230 Crystallographic Space Groups* (World Scientific, Singapore, 1988).
[46] R. D. Shannon, Acta Crystallogr. Sect. A **32**, 751 (1976).
[47] Although one might come up with a role for SOJT effects in inversion symmetry breaking because this series is titanates, the displacements of Ti ions make a small contribution to the distortion corresponding to the $M_1(\eta_1, \eta_1)$ mode, in sharp contrast to the zone-center polar modes driven by the SOJT effects in ferroelectric titanates such as $BaTiO_3$.
[48] T. Ozawa, A. Ikoshi, T. Taniguchi, S. Mizusaki, Y. Nagata, Y. Noro, and H. Samata, J. Alloys Compd. **448**, 38 (2008).
[49] Y. Kobayashi, M. Tian, M. Eguchi, and T. E. Mallouk, J. Am. Chem. Soc. **131**, 9849 (2009).
[50] F. Izumi and K. Momma, Solid State Phenom. **130**, 15 (2007).
[51] In the previous reports [28], the tetragonal $P\bar{4}2_1m$ space group has not been proposed, likely because the cell doubling was considered as a tetragonal-to-orthorhombic phase transition.
[52] S. A. Denev, T. T. A. Lummen, E. Barnes, A. Kumar, and V. Gopalan, J. Am. Ceram. Soc. **94**, 2699 (2011).
[53] B. B. Van Aken, T. T. M. Palstra, A. Filippetti, and N. A. Spaldin, Nat. Mater. **3**, 164 (2004).
[54] C. J. Fennie and K. M. Rabe, Phys. Rev. B **72**, 100103 (2005).
[55] The freezing of the $M_1(\eta_1, \eta_1)$ mode induces a nonpolar Γ_4^- mode by symmetry, while the K_3 mode induces a polar Γ_2^- mode in $YMnO_3$ [52,53].
[56] In contrast, hybrid improper ferroelectrics may have intermediate states with a condensation of one of the two modes coming together to lead to noncentrosymmetry [10].
[57] X. Wu, D. Vanderbilt, and D. R. Hamann, Phys. Rev. B **72**, 035105 (2005).
[58] Z. Wu and R. E. Cohen, Phys. Rev. Lett. **95**, 037601 (2005).
[59] K. Tezuka, Y. Hinatsu, N. M. Masaki, and M. Saeki, J. Solid State Chem. **138**, 342 (1998).
[60] H. J. Monkhorst and J. D. Pack, Phys. Rev. B **13**, 5188 (1976).
[61] D. Orobengoa, C. Capillas, M. I. Aroyo, and J. M. Perez-Mato, J. Appl. Crystallogr. **42**, 820 (2009).
[62] J. M. Perez-Mato, D. Orobengoa, and M. I. Aroyo, Acta Crystallogr. Sect. A **66**, 558 (2010).
[63] J. Brous, I. Fankuchen, and E. Banks, Acta Crystallogr. **6**, 67 (1953).
[64] H. T. Stokes and B. J. Campbell, Isotropy Software Suite, http://stokes.byu.edu/iso/isotropy.php.
[65] H. T. Stokes, B. J. Campbell, and R. Cordes, Acta Crystallogr. Sect. A **69**, 388 (2013).